INTERNATIONAL JOURNAL OF REMOTE SENSING, 2016
VOL. 37, NO. 4, 926–949
http://dx.doi.org/10.1080/01431161.2016.1143136

Taylor & Francis
Taylor & Francis Group

Land cover post-classifications by Markov chain geostatistical cosimulation based on pre-classifications by different conventional classifiers

Weixing Zhang, Weidong Li and Chuanrong Zhang

Department of Geography and Center for Environmental Sciences and Engineering, University of Connecticut, Storrs, CT 06269, USA

ABSTRACT

The recently proposed Bayesian Markov chain random field (MCRF) cosimulation approach, as a new non-linear geostatistical cosimulation method, for land cover classification improvement (i.e. post-classification) may significantly increase classification accuracy by taking advantage of expert-interpreted data and pre-classified image data. The objective of this study is to explore the performance of the MCRF post-classification method based on pre-classification results from different conventional classifiers on a complex landscape. Five conventional classifiers, including maximum likelihood (ML), neural network (NN), Support Vector Machine (SVM), minimum distance (MD), and *k*-means (KM), were used to conduct land cover pre-classifications of a remotely sensed image with a 90,000 ha area and complex landscape. A sample dataset (0.32% of total pixels) was first interpreted based on expert knowledge from the image and other related data sources, and then MCRF cosimulations were performed conditionally on the expert-interpreted sample dataset and the five pre-classified image datasets, respectively. Finally, MCRF post-classification maps were compared with corresponding pre-classification maps. Results showed that the MCRF method achieved obvious accuracy improvements (ranging from 4.6% to 16.8%) in post-classifications compared to the pre-classification results from different pre-classifiers. This study indicates that the MCRF post-classification method is capable of improving land cover classification accuracy over different conventional classifiers by making use of multiple data sources (expert-interpreted data and pre-classified data) and spatial correlation information, even if the study area is relatively large and has a complex landscape.

ARTICLE HISTORY
Received 18 June 2015
Accepted 12 January 2016

1. Introduction

Rapid human modification of land cover (including land use) has transformed both global natural conditions and regional environments (Lambin et al. 2001; Lawrence and Chase 2010). Land cover is a key variable that has an impact on many parts of the human and physical environments. Thoroughly understanding the spatial distribution of different

CONTACT Chuanrong Zhang chuanrong.zhang@uconn.edu Department of Geography and Center for Environmental Sciences and Engineering, University of Connecticut, Storrs, CT 06269, USA

land cover classes is essential in the study of global and regional environments and their changes (Anderson et al. 1976; Loveland et al. 2000). Despite the significance of land cover as an important environmental variable, our knowledge of land cover and its dynamics is poor. Recently, remote sensing, as a cutting-edge technique, has provided abundant, reliable, and multi-temporal land cover data for earth observation at various spatial scales (Bruzzone, Prieto, and Serpico 1999; Mas 1999). Land cover classification using remotely sensed images has produced useful thematic maps for scientific study and social applications (Wilkinson 2005). However, land cover maps derived from remote-sensing imagery are often judged to be of insufficient quality for many applications because land cover classification is so complicated that many classifiers cannot produce accurate land cover maps due to reasons such as spectral confusion, complex landscape, and low quality of remote-sensing imagery (Lu and Weng 2007; Manandhar, Odeh, and Ancev 2009). For example, pixel-based classifiers, which are commonly used as sophisticated ways to perform land cover classifications, do not take spatial context information into account and, thus, often suffer from 'salt and pepper' noise. One reason for this may be that a pixel may involve multiple features if it is larger than the area of a specific feature; that is, a pixel may cover two or more feature classes due to the complicated biophysical environment (Shekhar et al. 2002; Lu and Weng 2007).

It is still challenging to make a high-quality land cover classification map, even though a large number of enhanced classification methods have been developed, such as support vector machines (Brown, Gunn, and Lewis 1999; Hsu and Lin 2002), geostatistical classifiers (Goovaerts 2002; Park, Chi, and Kwon 2003), knowledge-based algorithms (Dobson, Pierce, and Ulaby 1996; Schmidt et al. 2004), and hybrid classifiers (e.g. a combination of pixel-based classifier and object-based classifier) (De Jong, Hornstra, and Maas 2001; Debeir et al. 2002; Kuemmerle et al. 2006; Li, Meng, et al. 2013). In order to increase the accuracy of a land cover classification, those advanced approaches make extensive use of as much available information as possible, including geometrical information, spectral signature, image transformation, spatial or contextual information, and other available data (Lu and Weng 2007).

Post-classification operations are expected to be an effective way to improve the accuracy of a land cover classification. Significant effort has been devoted to developing various techniques for post-classification operations. In general, there can be two post-classification methods in land cover classification. One method is to remove noise or correct misclassified pixels through filters or moving windows based on expert systems, knowledge-based rules, texture information, or neighbourhood correlations. For example, Barnsley and Barr (1996) successfully applied a kernel-based spatial processing method to improve land use classification in urban areas. Knowledge-based processing was employed to conduct error correction at the post-classification stage by Murai and Omatu (1997) and Manandhar, Odeh, and Ancev (2009). The accuracy of urban building classification was improved significantly through combining unsupervised clustering and modified co-occurrence matrix-based filtering (Zhang 1999, 2001). Stefanov, Ramsey, and Christensen (2001) adopted an expert system to sort initial land cover classification results of central Arizona–Phoenix in the USA by using ancillary data. To improve land cover classification results from very-high-resolution images, Van de Voorde, De Genst, and Canters (2007) utilized several techniques including a shadow-removal technique, knowledge-based rules, and a region-based filter. Thapa and Murayama (2009) used a combination method, which first extracted similarly classified

pixels from land cover maps generated by three classifiers and then filled empty pixels using a fuzzy supervised approach, to conduct more accurate urban mapping.

The other method is to incorporate potentially useful spatial correlation information between a pixel and its neighbours and other helpful ancillary data into reclassifications using probabilistic or geostatistical models. This is an available and promising way to improve classification accuracy by incorporating spatial dependency information and multi-scale ancillary data with different reliabilities (Carvalho, Soares, and Bio 2006). For example, Vaiphasa, Skidmore, and De Boer (2006) applied a Bayesian probability-based classifier to increase the accuracy of mangrove maps using GIS data. Carvalho, Soares, and Bio (2006) increased the accuracy of some forest tree species classification by integrating reliable field data and pre-classified data using a direct sequential cosimulation algorithm. Tang et al. (2013) used a multiple-point geostatistical approach to increase the land cover classification accuracy by integrating multiple-point statistics extracted from a pre-classified image, pre-classification posterior probabilities, and training samples.

Recently, Li et al. (2015) proposed a Bayesian Markov chain random field (MCRF) cosimulation approach for improving land cover classification accuracy (i.e. a post-classification method) based on expert-interpreted sample data and pre-classified image data. A test using a simple example (a small area with simple landscape) has proven the efficacy of the MCRF post-classification method (Li et al. 2015). However, further studies are necessary to examine the applicability of this method to complex landscape situations with different pre-classification methods. In this study, we chose five widely used conventional classifiers to perform pre-classifications of a remotely sensed image for a relatively large area with a complex and varied landscape. Each pre-classified image dataset was then used together with an expert-interpreted sample dataset to conduct a post-classification operation by using the MCRF method. The objectives are to: (1) examine the performance of the MCRF method for land cover post-classification in a complex landscape environment, (2) explore how much the MCRF post-classification method can improve classification accuracy over the pre-classified results generated by different fast conventional classifiers, and (3) understand the impacts of these conventional classifiers for pre-classification on the final classification results.

2. Experimental data sets

2.1. *Image data*

A medium-resolution (Landsat 8 OLI) image for Wuhan, China, acquired on 17 September 2013, was used in this study. There are total 11 bands in the Landsat 8 OLI image, including all of the bands (blue, green, red, near-infrared, short-wave infrared 1, and short-wave infrared 2) from the previous Landsat missions. New band 1 (coastal aerosol) is designed for coastal and aerosol studies and new band 9 (cirrus) is designed for cirrus cloud detection (US Geological Survey 2012). Band 8 is a panchromatic band with a spatial resolution of 15 m. Bands 10 and 11 (thermal infrared) are for surface temperature detection with a spatial resolution of 100 m. Selecting the appropriate bands for use is important for the purpose of mapping. This study is to explore the

performance of the MCRF post-classification method based on land cover pre-classification results. Therefore, the six commonly used spectral bands (bands 2–7) of the image were extracted and stacked for pre-classification to facilitate data processing.

A scene of 1000 rows by 1000 columns with a spatial resolution of 30 m, which covers the northeastern part of Wuhan with an area of 90,000 ha, was clipped from the image as the study area (Figure 1). The study area has a relatively heterogeneous and complex landscape, comprising urban areas, suburb areas, agricultural lands, rivers, hills, woodlands, and many water bodies (lakes and ponds), with rugged topography. For this study, five major land cover classes were mapped, namely, built-up area, farmland, woodland, waterbody, and bare land (Table 1).

2.2. *Expert-interpreted data*

In this study, the MCRF post-classification method was employed to make use of both pre-classification data and expert-interpreted data in order to improve the accuracy of land cover classification. A total of 4021 data points were interpreted by expert judgement based on professional insight, through integrating information from multiple sources, including high-resolution aerial images and other reliable reference data, such as Baidu Maps (map.baidu.com), Bing Maps (www.bing.com/maps), and Google Earth

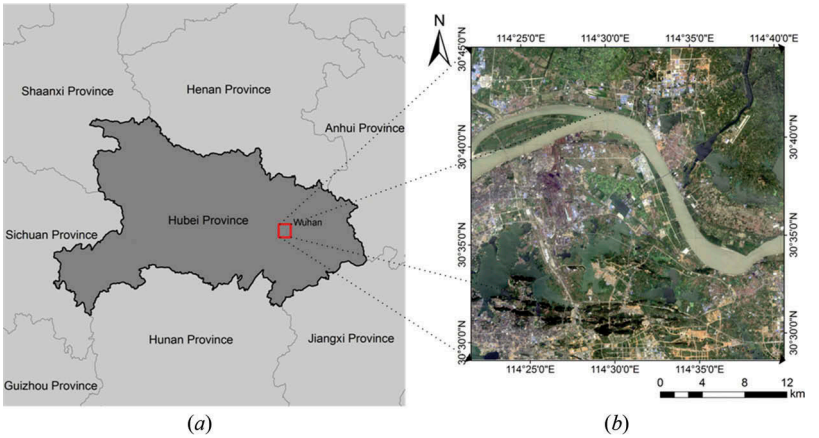

Figure 1. The Landsat 8 OLI true colour image (**b**) (R: red, G: green, B: blue) for the study area in Wuhan, Hubei Province (**a**), China. The image was acquired on 17 September 2013, with a pixel size of 30 m × 30 m. The latitude and longitude of the upper left corner of the image are 30°45′04″ N and 114°22′13″ E, respectively.

Table 1. Description of related land cover classes.

Class	Class symbol	Description
Built-up area	C1	Industrial, commercial, residential areas or other areas with manmade facilities
Farmland	C2	Arable land that is used to plant crops
Woodland	C3	Land that is mostly covered with woods or dense growths of trees and shrubs
Waterbody	C4	Earth surface covered with water, for example, lake, river, and pond.
Bare land	C5	Land that is bare without any cover

historical imagery (www.google.com/earth), as well as existing local land cover/use maps. The expert-interpreted data were then split into two groups. In total, 3215 points (0.32% of the total image pixels in the study area) were used as conditioning sample data (i.e. hard data) in cosimulation (Figure 2a), and the remaining 806 points were used for validation (Figure 2b). The expert-interpreted data cannot be used as training data for pre-classification because they are interpreted from multiple sources mentioned earlier and thus may not reflect the typical spectra of the image used for pre-classification. Training data for pre-classification were discerned only from the original remotely sensed image of the study area selected for pre-classification. Specific quantities of expert-interpreted sample data, validation data, and training data for each land cover class are given in Table 2.

3. Methods

3.1. *Basic procedure*

Five conventional classifiers, including maximum likelihood (ML), neural network (NN), Support Vector Machine (SVM), minimum distance (MD), and *k*-means (KM), were used to produce pre-classified land cover maps. In order to sufficiently utilize the spectral information for supervised classifications (i.e. to obtain pre-classification maps with relatively high accuracies from the selected image purely based on spectral data), each land cover class was represented by representative samples. The same training

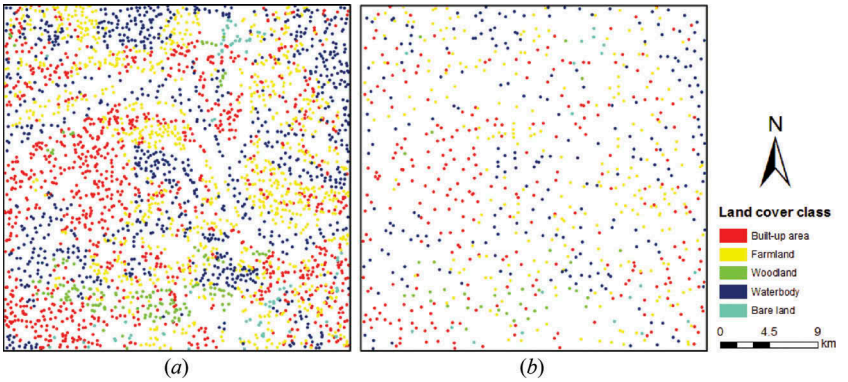

Figure 2. Expert-interpreted data: 3215 points for MCRF cosimulation (**a**), and 806 points for validation (**b**) .

Table 2. Quantities of expert-interpreted sample data for post-classification operations, expert-interpreted validation data for classification accuracy estimation, and training data for pre-classifications.

Class	Expert-interpreted sample data (pixels)	Validation data (pixels)	Training data (pixels)
Built-up area	1114	280	470
Farmland	997	250	331
Woodland	142	35	88
Waterbody	889	222	333
Bare land	73	19	60

data were utilized for the first four supervised classifiers. Spectral separability of the training data for different land cover classes was estimated using Jeffries–Matusita distance analysis in order to select proper training samples. Values of Jeffries–Matusita distance analysis greater than 1.9 indicate that the land cover pairs have relatively good separability. The values of Jeffries–Matusita distance analysis for the finally selected training data used in this study ranged from 1.89 to 2.00 (Table 3). Post-classifications by the MCRF method were conducted on the pre-classified data and expert-interpreted sample data.

ENVI software was used to perform the ML, NN, SVM, and MD pre-classifications and ERDAS Imagine was used for the KM pre-classification. For the MCRF post-classifications, FORTRAN and Python computer codes were used.

3.2. *Image post-classification*

3.2.1. *Markov chain random fields*

The MCRF cosimulation algorithm is an extension of the MCRF sequential simulation algorithm based on the MCRF theory, which was initially proposed by Li (2007a) as the supporting theory of Markov chain geostatistics and further described with emphasis on the Bayesian updating view in Li, Zhang, et al. (2013, 2015). An MCRF is a spatial Markov chain that runs in a space and at any unobserved location decides its state by interacting with nearest data through Bayesian updating. The local conditional probability distribution of an MCRF at any unobserved location is decided by a sequential Bayesian updating process of the prior probability using each of the nearest data within a neighbourhood as new evidence.

The MCRF local conditional probability function for a specific unobserved location (here, a location means the centroid of a pixel) $\boldsymbol{u}_0$ is described as

$$P[i_0(\boldsymbol{u}_0)|i_1(\boldsymbol{u}_1),\ldots,i_m(\boldsymbol{u}_m)] = \frac{P[i_m(\boldsymbol{u}_m)|i_0(\boldsymbol{u}_0),\ldots,i_{m-1}(\boldsymbol{u}_{m-1})]\cdots P[i_2(\boldsymbol{u}_2)|i_0(\boldsymbol{u}_0)i_1(\boldsymbol{u}_1)]P[i_0(\boldsymbol{u}_0)|i_1(\boldsymbol{u}_1)]}{P[i_1(\boldsymbol{u}_1),\ldots,i_m(\boldsymbol{u}_m)]/P[i_1(\boldsymbol{u}_1)]}, \quad (1)$$

where $\boldsymbol{u}$ represents the location vector (i.e. coordinates) of a pixel, i_0 refers to the land cover class of the unobserved pixel at location $\boldsymbol{u}_0$, i_1 to i_m denote the classes of the m nearest data neighbours (i.e., label-informed pixels) around $\boldsymbol{u}_0$, and P indicates a probability or conditional probability.

Assuming conditional independence of nearest data within a neighbourhood and using the transiogram notation (Li 2007b), as well as applying the total probably law, Equation (1) is simplified to

Table 3. Spectral separability of training data for pre-classifications.

Class	Built-up area	Farmland	Woodland	Waterbody	Bare land
Built-up area		1.8899	1.9991	1.9833	1.9562
Farmland			1.8905	1.9450	1.9814
Woodland				1.9900	2.0000
Waterbody					1.9999
Bare land					

$$P[i_0(\boldsymbol{u}_0)|i_1(\boldsymbol{u}_1),\ldots,i_m(\boldsymbol{u}_m)] = \frac{P_{i_1 i_0}(\mathbf{h}_{10})\prod_{g=2}^{m} P_{i_0 i_g}(\mathbf{h}_{0g})}{\sum_{f_0=1}^{n}[P_{i_1 f_0}(\mathbf{h}_{10})\prod_{g=2}^{m} P_{f_0 i_g}(\mathbf{h}_{0g})]}, \quad (2)$$

where ∑ is a summation symbol, n is the number of classes, f_0 refers to all of the possible classes of the unobserved pixel at location $\boldsymbol{u}_0$, Π is a multiplication symbol, and $P_{i_0 i_g}(\mathbf{h}_{0g})$ is a specific transition probability over the specific separation distance $\mathbf{h}_{0g}$ between locations $\boldsymbol{u}_0$ and $\boldsymbol{u}_g$, which can be fetched from a transiogram model $P_{i_0 i_g}(\mathbf{h})$.

A transiogram is theoretically defined as a two-point transition (or conditional) probability function over the separation distance:

$$P_{ij}(\mathbf{h}) = P[\mathrm{Z}(\boldsymbol{u}+\mathbf{h}) = j|\mathrm{Z}(\boldsymbol{u}) = i], \quad (3)$$

where i and$j$ denote the specific classes of random variables $\mathrm{Z}(\boldsymbol{u})$ and $\mathrm{Z}(\boldsymbol{u}+\mathbf{h})$ at locations $\boldsymbol{u}$ and $\boldsymbol{u}+\mathbf{h}$, respectively; and $\mathbf{h}$ denotes the separation distance between locations $\boldsymbol{u}$ and $\boldsymbol{u}+\mathbf{h}$. With increasing $\mathbf{h}$, values of $P_{ij}(\mathbf{h})$ form a transition probability curve. Transiogram models can be inferred from experimental transiograms that are directly estimated from sample data globally (Li 2007b).

3.2.2. *MCRF cosimulation*

To approximately meet the conditional independence condition of nearest data, the MCRF sequential simulation algorithm uses a quadrantal neighbourhood, which considers only one nearest datum from each quadrant that sectors the neighbourhood (Li and Zhang 2007). The MCRF cosimulation algorithm for improving land cover classification considers the co-located datum of a covariate field, namely, a pre-classified image, into its local conditional probability function. Therefore, the MCRF cosimulation model for improving land cover classification is given as

$$P[i_0(\boldsymbol{u}_0)|i_1(\boldsymbol{u}_1),\ldots,i_4(\boldsymbol{u}_4);r_0(\boldsymbol{u}_0)] = \frac{Q_{i_0 r_0}P_{i_1 i_0}(\mathbf{h}_{10})\prod_{g=2}^{4} P_{i_0 i_g}(\mathbf{h}_{0g})}{\sum_{f_0=1}^{n}[Q_{f_0 r_0}P_{i_1 f_0}(\mathbf{h}_{10})\prod_{g=2}^{4} P_{f_0 i_g}(\mathbf{h}_{0g})}, \quad (4)$$

where $Q_{i_0 r_0}$ represents the cross-field transition probability from class i_0 at location $\boldsymbol{u}_0$ in the random field being simulated to class r_0 at the co-location in the auxiliary field – the pre-classified image (Li et al. 2015).

3.2.3. *Inputs and outputs of MCRF cosimulations*

Besides expert-interpreted sample data and pre-classified image data, two sets of parameter data are required in the MCRF cosimulation algorithm for land cover post-classification. They are transiogram models and the cross-field transition probability matrix (Li et al. 2015). Transiogram models are used to represent the spatial auto and cross correlations of classes in the field to be simulated and they can be inferred from experimental transiograms that are directly estimated from sample data (Li 2007b). Transiogram model joint inference may be done using two methods – the mathematical model method and the linear interpolation method (Li and Zhang 2010). In this study, because we have sufficient expert-interpreted sample data to generate reliable experimental transiograms, we used the efficient linear interpolation method to obtain the entire set of transiogram models. The cross-field transition probability matrix represents the correlations between classes of the field being simulated and the classes of the pre-classified image, and it can be simply

estimated using the transitions from the sample data set to their corresponding co-located data in the pre-classified image (Li, zhang, et al. 2013).

The five conventional classifiers aforementioned were used to pre-classify the selected remotely sensed image to obtain five pre-classified image datasets for use in the MCRF post-classification operations. A total of 100 simulated realizations were generated for each cosimulation case (there are a total of five cases for different pre-classifications based on different conventional classifiers in this study), and an optimal classification map was further obtained according to the maximum probabilities estimated from the set of simulated realizations. The accuracy of each optimal classification map was calculated using the validation sample dataset. By comparing with those pre-classification results, classification accuracy improvements made by post-classification operations were finally available.

4. Results

4.1. *Improvement over maximum likelihood classification*

A comparison of classification accuracies between the pre-classification by the ML classifier and the post-classification by MCRF cosimulation is presented in Table 4. The overall accuracy (OA) and kappa coefficient (κ) of the ML pre-classification map are 81.9% and 0.762, respectively. However, the OA and κ for the MCRF post-classification map are 86.6% and 0.820, respectively. Apparent improvement in land cover classification accuracy is made by the MCRF method. In the pre-classification map, the misclassifications among the five classes are explainable by spectral confusion (e.g. some built-up area pixels were misclassified into farmland and bare land, and some farmland pixels were misclassified into woodland). After post-processing by MCRF cosimulation, there are obvious increases in the producer's accuracies of built-up area (from 72% to 78%), farmland (from 83% to 90%), and woodland (from 83% to 91%). Checking the user's accuracies, one can see that significant improvements for woodland (from 50% to 78%) and bare land (from 45% to 94%) were made by the post-classification. In addition, before post-classification was made, much noise (i.e. 'pepper and salt effect') in the pre-classification map (Figure 3a) can be seen. This noise is likely a result of spectral confusion due to lack of spectral separability among some land cover classes in the study area. After post-classification, the 'salt and pepper' noise, which is a common problem for pixel-based classifications, is mostly removed by the MCRF method (Figure 3b). A drawback is that linear features (e.g. roads), which were partially captured by the pre-classification, were mostly lost in the MCRF post-classification process.

4.2. *Improvement over neural network classification*

Table 5 and Figure 4 present the pre-classification results by the NN classifier and the corresponding post-classification results by the MCRF method. Compared with the NN pre-classification, classification accuracy improvement made by the MCRF post-classification is notably large, with 10.4% increase in OA and 0.128 increase in the κ. In the pre-classification map, woodland was strongly overestimated, and the other two land cover classes, namely, bare land and built-up area, were also overestimated to some extent,

Table 4. Accuracy assessment for ML pre-classification and corresponding MCRF post-classification.

ML pre-classification							
	Validation data						
Class	C1	C2	C3	C4	C5	Total	User's Accuracy (%)
C1	201	6	0	6	3	216	93
C2	64	209	5	9	1	288	73
C3	0	28	29	1	0	58	50
C4	0	4	1	206	0	211	98
C5	15	3	0	0	15	33	45
Total	280	250	35	222	19	806	
Producer's Accuracy (%)	72	84	83	93	79		81.9
Overall Accuracy: 81.9%. kappa coefficient: 0. 762							
Improvement in overall accuracy: 4.7%. Improvement in kappa coefficient: 0.058							

MCRF post-classification							
	Validation data						
Class	C1	C2	C3	C4	C5	Total	User's Accuracy (%)
C1	219	15	1	1	3	239	92
C2	57	224	2	13	1	297	75
C3	1	8	32	0	0	41	78
C4	2	3	0	208	0	213	98
C5	1	0	0	0	15	16	94
Total	280	250	35	222	19	806	
Producer's Accuracy (%)	78	90	91	94	79		86.6
Overall Accuracy: 86.6%. kappa coefficient: 0.820							

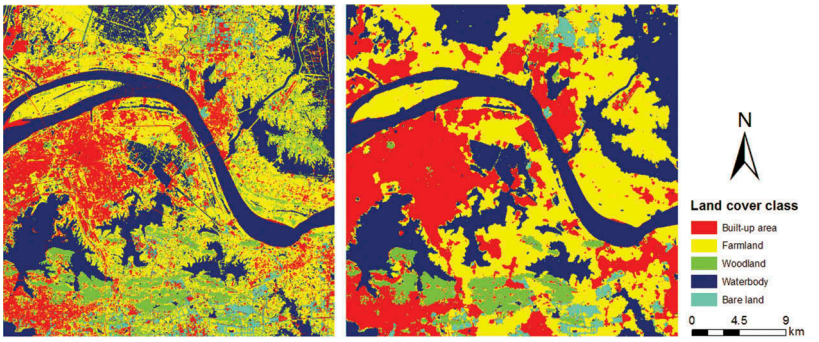

Figure 3. ML pre-classification (**a**) and corresponding MCRF post-classification (**b**) .

based on the spectral signatures derived from the remotely sensed image, while farmland and waterbody were underestimated (Table 5). Much farmland in the NN pre-classified map (Figure 4a) was misclassified into woodland, and a portion of farmland was also misclassified as built-up area, thus resulting in low producer's accuracy (57%) for farmland and low user's accuracy (30%) for woodland. Low user's accuracy (48%) also occurred for the bare land in the NN pre-classification map due to the misclassification of some built-up area and farmland pixels. Before post-classification, some of waterbody pixels were misclassified as farmland and built-up area because they were spectrally confused because some waterbody areas in the study area were covered by dense water plants. The MCRF post-classification operation changed this situation by correcting most misclassifications, except that some build-up area pixels were misclassified into farmland, causing some decreases in the producer's accuracy of built-up area and the user's accuracy of farmland. Similarly, linear features (mainly roads) were not captured, while most noise was removed in the post-classification map.

4.3. *Improvement over Support Vector Machine classification*

The pre-classification of the remotely sensed image by the SVM classifier has a relative higher OA and κ compared to that by NN, although the same training data were used. SVM generally performed poorly in separating built-up area from farmland, so that built-up area has a low producer's accuracy of 65% and farmland has a low user's accuracy of 62%. It also could not effectively separate waterbody from farmland, thus leading to a relatively low producer's accuracy for waterbody (82%) (Table 6). Before MCRF cosimulation was applied, some waterbody pixels were misclassified as farmland, and some built-up area pixels were also misclassified into farmland (Figure 5a). The former problem should be caused by the spectral confusion between waterbody and farmland because some waterbody areas in the study area were covered by dense water plants. The latter problem also occurred in the ML pre-classification. After post-processing by MCRF cosimulation, most of misclassified waterbody pixels (which were misclassified into farmland in pre-classification) were corrected with the help of the post-classification (Figure 5b). However, some correctly classified farmland in the pre-classification map was mistakenly changed to built-up area and waterbody in the post-classification map. This problem may be attributed to the smoothing

Table 5. Accuracy assessment for NN pre-classification and corresponding MCRF post-classification.

NN pre-classification							
	Validation data						
Class	C1	C2	C3	C4	C5	Total	User's Accuracy (%)
C1	245	39	0	16	1	301	81
C2	15	142	4	16	3	180	79
C3	6	60	31	6	0	103	30
C4	3	4	0	184	0	191	96
C5	11	5	0	0	15	31	48
Total	280	250	35	222	19	806	
Producer's Accuracy (%)	88	57	89	83	79		76.6
Overall Accuracy: 76.6%. kappa coefficient: 0. 697							
Improvement in overall accuracy: 10.4%. Improvement in kappa coefficient: 0.128							

MCRF post-classification							
	Validation data						
Class	C1	C2	C3	C4	C5	Total	User's Accuracy (%)
C1	227	13	0	1	2	243	93
C2	50	227	2	24	0	303	75
C3	1	5	33	0	0	39	85
C4	1	5	0	197	0	203	97
C5	1	0	0	0	17	18	94
Total	280	250	35	222	19	806	
Producer's Accuracy (%)	81	91	94	89	89		87.0
Overall Accuracy: 87.0%. kappa coefficient: 0.825							

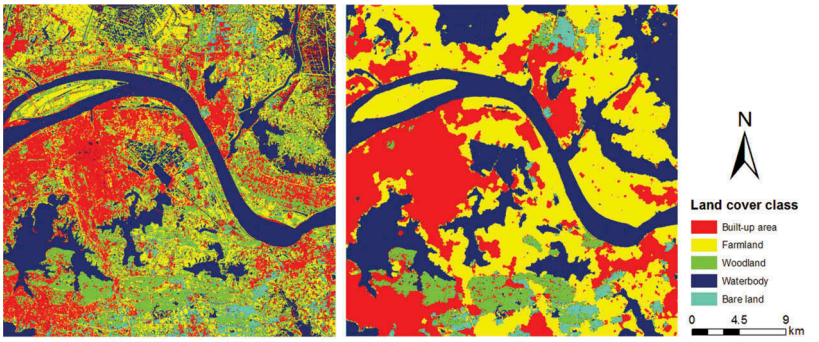

Figure 4. NN pre-classification (**a**) and corresponding MCRF post-classification (**b**) .

effect in the optimal classification map and the filtering effect caused by incorporation of spatial correlations in the MCRF cosimulation model. Because built-up area, farmland, and waterbody are the major land cover classes in this study, their conjunction probabilities were relatively high sometimes. Even so, the post-classification by the MCRF method increased the OA by 4.6% and κ by 0.057. Specifically, post-classification improved the producer's accuracies of built-up area, woodland, waterbody, and bare land by 11%, 6%, 13%, and 5%, respectively (with 10% accuracy decrease for farmland) (Table 6), and also increased the user's accuracy of farmland by 11%, finally yielding a less dispersed land cover class map. The filtering effect of the MCRF post-classification method to noise was clear, despite its inability to capture linear features as a common problem of two-point spatial statistical models (Figure 5b).

4.4. *Improvement over minimum distance classification*

The OA of the MD pre-classification (Figure 6a) is the lowest (67.1%) compared with the OAs of the pre-classified images by other conventional classifiers. This is because of the nature of the MD classifier, which generally has good performance when the distance between the mean values of every pair of classes is large compared with the variance of each class with respect to its mean. The MD classifier has a certain limitation if the spectral variance of each class is large, because it is insensitive to different degrees of spectral variance. In this case, the low classification accuracy of the MD pre-classification can be explained by the complex landscape, which has much higher spectral confusion among different land cover classes. As shown in Table 7, almost half of the built-up area and bare land in the image was classified wrongly by MD. Before MCRF post-classification was applied, some waterbody pixels were misclassified as farmland due to the spectral confusion between them caused by dense water plants in some waterbodies. The MCRF post-classification greatly changed the pre-classification results (Figure 6b). The OA in the post-classification map reached 83.9% with a remarkable improvement of 16.8%, although the co-image (i.e. the pre-classified image used as an auxiliary dataset) had a low accuracy (67.1%). Both producer's accuracies and user's accuracies of all land cover classes were increased to some extent after MCRF post-classification.

Table 6. Accuracy assessment for SVM pre-classification and corresponding MCRF post-classification.

SVM pre-classification							
	Validation data						
Class	C1	C2	C3	C4	C5	Total	User's Accuracy (%)
C1	183	10	0	1	0	194	94
C2	94	233	5	38	4	374	62
C3	0	5	30	1	0	36	83
C4	2	1	0	182	0	185	98
C5	1	1	0	0	15	17	88
Total	280	250	35	222	19	806	
Producer's Accuracy (%)	65	93	86	82	79		79.8
Overall Accuracy: 79.8%. kappa coefficient: 0. 736							
Improvement in overall accuracy: 4.6%. Improvement in kappa coefficient: 0.057							

MCRF post-classification							
	Validation data						
Class	C1	C2	C3	C4	C5	Total	User's Accuracy (%)
C1	213	19	1	0	2	235	91
C2	61	209	2	12	1	285	73
C3	1	7	32	0	0	40	80
C4	4	12	0	210	0	226	93
C5	1	3	0	0	16	20	80
Total	280	250	35	222	19	806	
Producer's Accuracy (%)	76	84	91	95	84		84.4
Overall Accuracy: 84.4%. kappa coefficient: 0.793							

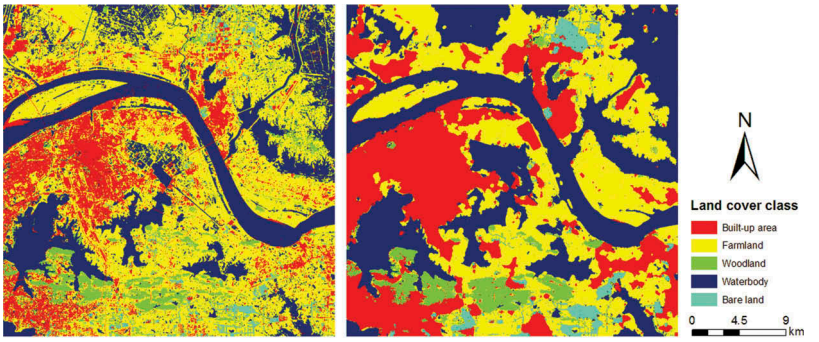

Figure 5. SVM pre-classification (**a**) and corresponding MCRF post-classification (**b**) .

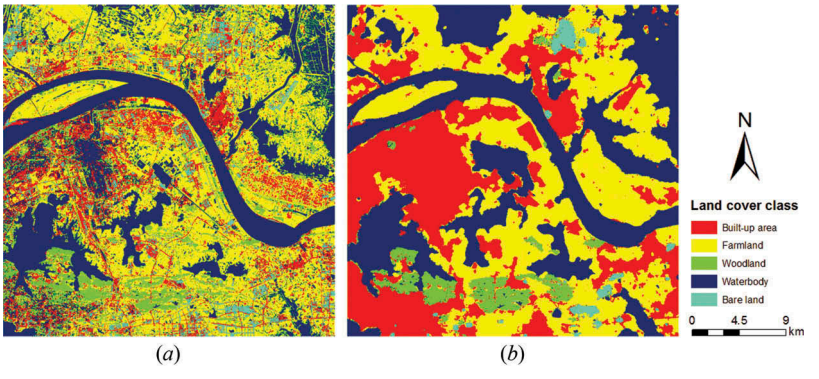

Figure 6. MD pre-classification (**a**) and corresponding MCRF post-classification (**b**) .

4.5. *Improvement over k-means classification*

In the pre-classification map produced by the unsupervised KM classifier, farmland was not well distinguished from built-up area and woodland, and waterbody was not well separated from farmland and woodland (Table 8, Figure 7). This means they had some spectral characteristics in common. Similar to the classifications by other conventional methods except for SVM, the KM pre-classification has quite low user's accuracy for woodland, because some pixels of farmland and waterbody were misclassified as woodland. The reason for these problems may be because crops, water plants, and urban vegetation have similar image digital number values in the remotely sensed image used for pre-classification. In addition, many built-up area pixels were misclassified into bare land, which means some built-up area and some bare land could not be effectively separated by the KM classifier. With the help of expert-interpreted ancillary data and the pre-classification image based on KM, the MCRF post-classification greatly increased the OA from 69.1% to 85.9% and the κ from 0.612 to 0.811 (Table 8). However, the producer's accuracy of built-up area had little improvement, and the user's accuracy of farmland also did not improve much, because some built-up area pixels were misclassified into farmland in the post-classification map. This may be explained by the smoothing effect normally shown in the optimal classification map and the filtering effect of the

Table 7. Accuracy assessment for MD pre-classification and corresponding MCRF post-classification.

MD pre-classification							
	Validation data						
Class	C1	C2	C3	C4	C5	Total	User's Accuracy (%)
C1	149	29	0	1	7	186	80
C2	30	195	5	57	1	288	68
C3	11	15	30	8	0	64	47
C4	46	4	0	156	0	206	76
C5	44	7	0	0	11	62	18
Total	280	250	35	222	19	806	
Producer's Accuracy (%)	53	78	86	70	58		67.1
Overall Accuracy: 67.1%. kappa coefficient: 0.592							
Improvement in overall accuracy: 16.8%. Improvement in kappa coefficient: 0.194							

MCRF post-classification							
	Validation data						
Class	C1	C2	C3	C4	C5	Total	User's Accuracy (%)
C1	213	14	0	4	6	237	90
C2	60	221	2	21	1	305	72
C3	1	4	33	0	0	38	87
C4	4	11	0	197	0	212	93
C5	2	0	0	0	12	14	86
Total	280	250	35	222	19	806	
Producer's Accuracy (%)	76	88	94	89	63		83.9
Overall Accuracy: 83.9%. kappa coefficient: 0.786							

Table 8. Accuracy assessment for KM pre-classification, and corresponding MCRF post-classification.

KM pre-classification							
	Validation data						
Class	C1	C2	C3	C4	C5	Total	User's Accuracy (%)
C1	218	55	0	5	7	285	76
C2	2	153	3	57	0	215	71
C3	4	33	32	18	0	87	37
C4	8	0	0	142	0	150	95
C5	48	9	0	0	12	69	17
Total	280	250	35	222	19	806	
Producer's Accuracy (%)	78	61	91	64	63		69.1
Overall Accuracy: 69.1%. kappa coefficient: 0.612							
Improvement in overall accuracy: 16.8%. Improvement in kappa coefficient: 0.199							

MCRF post-classification							
	Validation data						
Class	C1	C2	C3	C4	C5	Total	User's Accuracy (%)
C1	220	10	0	0	5	235	94
C2	56	224	2	21	0	303	74
C3	1	5	33	0	0	39	85
C4	2	10	0	201	0	213	94
C5	1	1	0	0	14	16	88
Total	280	250	35	222	19	806	
Producer's Accuracy (%)	79	90	94	91	74		85.9
Overall Accuracy: 85.9%. kappa coefficient: 0.811							

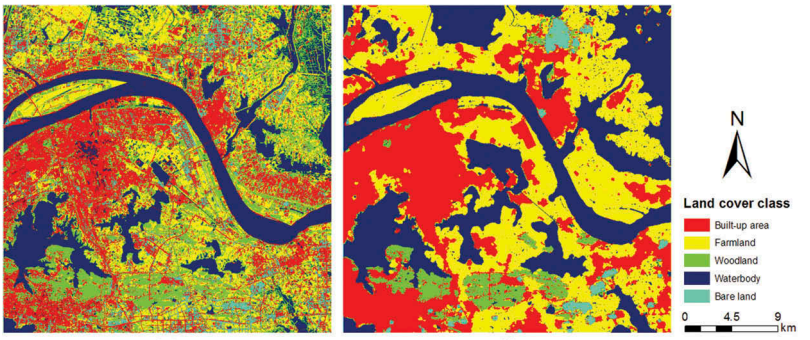

Figure 7. KM pre-classification (**a**) and corresponding MCRF post-classification (**b**) .

MCRF method, which caused some small fragments (one to a few pixels) of built-up area within large farmland patches to be classified wrongly into farmland. However, as shown in Table 8, the classification improvements for farmland, woodland, waterbody, and bare land were apparent in both producer's accuracies and user's accuracies, after post-classification was applied. A special feature for the KM pre-classification (Figure 7a) is that it shows better ability in extracting linear features (e.g. road and highway) than the other four classifiers due to manual reclassification in the second step of the method. But this did not contribute more to the MCRF post-classification because the two-point statistics-based MCRF model used here cannot capture linear features.

4.6. *Comparison of different post-classification cases*

Data in Table 9 summarize the results of the five pre-classification and post-classification pairs, which indicate that the MCRF method indeed can largely improve the accuracy of land cover classification through post-classification, no matter which of the five conventional

Table 9. Overall accuracy improvements of MCRF post-classifications over different pre-classifications of land cover classes.

			Producer's Accuracy (%)					User's Accuracy (%)				
			Class									
	Overall accuracy (%)	kappa coefficient	C1	C2	C3	C4	C5	C1	C2	C3	C4	C5
ML pre-classification	81.9	0.762	72	84	83	93	79	93	73	50	98	45
Post-classification	86.6	0.820	78	90	91	94	79	92	75	78	98	94
Improvement	4.7	0.058	6	6	9	1	0	−1	3	28	0	48
NN pre-classification	76.6	0.697	88	57	89	83	79	81	79	30	96	48
Post-classification	87.0	0.825	81	91	94	89	89	93	75	85	97	94
Improvement	10.4	0.128	−6	34	6	6	11	12	−4	55	1	46
SVM pre-classification	79.8	0.736	65	93	86	82	79	94	62	83	98	88
Post-classification	84.4	0.793	76	84	91	95	84	91	73	80	93	80
Improvement	4.6	0.057	11	−10	6	13	5	−4	11	−3	−5	−8
MD pre-classification	67.1	0.592	53	78	86	70	58	80	68	47	76	18
Post-classification	83.9	0.786	76	88	94	89	63	90	72	87	93	86
Improvement	16.8	0.194	23	10	9	18	5	10	5	40	17	68
KM pre-classification	69.1	0.612	78	61	91	64	63	76	71	37	95	17
Post-classification	85.9	0.811	79	90	94	91	74	94	74	85	94	88
Improvement	16.8	0.199	1	28	3	27	11	17	3	48	0	70

classifiers was used for pre-classification. Among the five conventional classifiers used for pre-classification, ML generated the highest OA, while MD produced the lowest. The overall accuracies of pre-classifications by the conventional classifiers are 81.9% (ML), 79.8% (SVM), 76.6% (NN), 69.1% (KM), and 67.1% (MD) in a descending sequence. The MCRF post-classification method increased the OAs by 4.7% over the ML classifier, 10.4% over the NN classifier, 4.6% over the SVM classifier, 16.8% over the MD classifier and the KM classifier, with an accuracy improvement sequence of SVM < ML < NN < MD = KM. In general, the lower the pre-classification accuracy, the higher the MCRF post-classification improvement will be. In some cases, MCRF post-classification caused some negative effects in classification accuracies of individual land cover classes, which mostly occurred in user's accuracies, especially for the post-classification case on the SVM pre-classification. However, these negative effects are negligible in comparison with the positive effects.

Except for the SVM pre-classification, minor land cover classes, namely, bare land and woodland, had very low user's accuracies (less than 50%) in pre-classifications. However, the MCRF method largely improved their user's accuracies in post-classifications. Improvements range from 46% to 70% for bare land, and from 28% to 55% for woodland. This means that most conventional classifiers have difficulties to accurately classify minor land cover classes, but the MCRF post-classification method can largely solve this problem.

Comparing all of the post-classifications with all of the corresponding pre-classifications, one can find that, in addition to classification accuracy improvement, the MCRF post-classification results have some other common characteristics, which are all essentially related with the smoothing effect of the MCRF cosimulation model:

(1) The MCRF post-classifications removed most 'salt and pepper' noise that appeared in pre-classification maps. This means that the MCRF method has the filtering effect to noise.
(2) Fine linear features appearing in pre-classification maps mostly disappeared in post-classification maps. These very narrow linear features in pre-classification maps were fragments of linear ground objects (mostly roads, and some ridges between lotus pools), partially captured by conventional classifiers. This means that the MCRF post-classification method cannot capture fine linear features. This inability should be common to two-point statistics-based spatial models.
(3) In the post-classifications, there were always some built-up area pixels to be misclassified into farmland, and in most cases there were also some waterbody pixels to be misclassified into farmland. This problem should be caused by the smoothing effect attached with the MCRF post-classification maps, which removed those isolated small built-up area or waterbody patches (as single pixels or clusters of only a few pixels) within large farmland patches.

5. Discussions

5.1. *Smoothing effect*

The MCRF post-classification method shows apparent smoothing effect in post-classified results. The smoothing effect includes the filtering effect of spatial models through

incorporating data dependency, and the smoothing effect caused by optimization for obtaining an optimal classification map. The former is caused by the neighbourhoods and two-point spatial measures used by spatial statistical methods, which cannot effectively capture (or can remove) linear features. This is because the neighbourhood of spatial statistical models uses data in a round area (e.g. circle, ellipse, or even square, in two dimensions), which is normally much wider than many narrow linear features. Thus, estimated values on a linear feature based on the data in a neighbourhood (if it is much wider than the linear feature) often reflect the classes outside the linear feature's area, consequently erasing the narrow linear features. It is widely known that two-point spatial measures cannot capture curvilinear features. This is the major smoothing effect responsible for losing linear features, and also the major reason for filtering noise. Multiple-point statistical methods may be better in capturing curvilinear features, but it only can approximately reproduce the known and relatively simple patterns from a fed training image (see Tang et al. 2013).

The smoothing effect caused by optimization for obtaining an optimal classification map based on maximum probabilities estimated from a number of simulated realisation maps is widely known in spatial statistics. In this study, because we used the optimal classification map as the final post-classification map, this smoothing effect also exists, but it does not hide the filtering effect of spatial statistical models. Figure 8 displays a part of the MCRF post-classification map based on the NN pre-classification and some other simulated results. The simulated realization map (Figure 8e) apparently shows more details than the optimal map (Figure 8d) does. The occurrence probability map of built-up area (Figure 8f) demonstrates the uncertainty of built-up area among different simulated realization maps, which reflects the credibility of built-up area in the optimal map. This means that the optimal map, that is, the post-classification map shown in this paper, has smoothing effect caused by the optimization. However, the simulated realization map still shows strong smoothing effect to the pre-classification map (Figure 8c), which filters out both noise and linear features. This smoothing or filtering effect carried by simulated realizations should be attributed to the neighbourhoods and two-point spatial measures of spatial statistical models.

5.2. *Comparison with the majority spatial filter*

The MCRF cosimulation model used in this study for post-classification is different from ordinary filters for filtering noise. Post-classification by a spatial filter with a moving window can remove some noise, and the filtering effect depends on the size of the local window (or neighbourhood). Such smoothing methods sometimes may improve classification results a little, but sometimes may not improve the results at all or even cause a decrease in accuracy. This is because such filtering methods do not incorporate new supportive information into the post-classifications, unless a specific expert system is combined with the filter. However, the major purpose of the MCRF post-classification method is to improve classification accuracy by incorporating expert-interpreted data from multiple data sources and spatial correlation information into post-classification operations. Of course, filtering noise is a common capability of spatial statistical models due to their incorporation of spatial dependency.

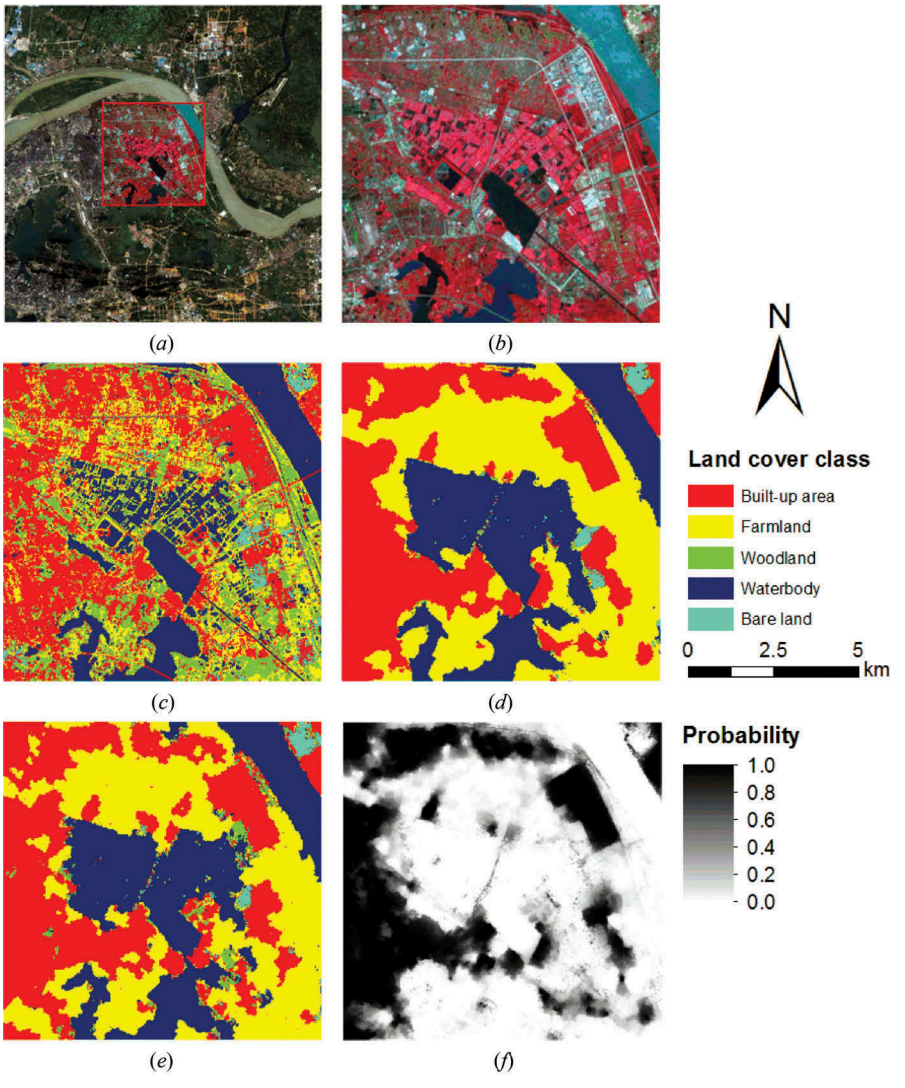

Figure 8. The Landsat 8 OLI true colour image of the study area (**a**), the enlarged false colour image of a subarea (**b**), corresponding NN pre-classification map (**c**), corresponding optimal map of MCRF post-classification (**d**), one simulated realisation of MCRF post-classification (**e**), and corresponding occurrence probability map of built-up area (**f**). The latitude and longitude of the upper left corner of the enlarged image are 30°40′09″N and 114°27′32″E, respectively.

We tested a majority spatial filter with 3 × 3 and 7 × 7 window sizes. Our results (Figure 9) showed that the effect of the filter is limited: It does filter out isolated pixels and small pixel groups, and the filtering effect strengthens with increasing window size (Figure 9d and 9e), but it does not improve accuracy in general (sometimes produces a small increase, and sometimes a small decrease). This is because it does not incorporate credible information from other sources to correct the misclassified pixels (e.g. the misclassified pixels from water-body to built-up area and woodland in Figure 9c). However, the MCRF cosimulation model corrected the misclassifications (Figure 9f).

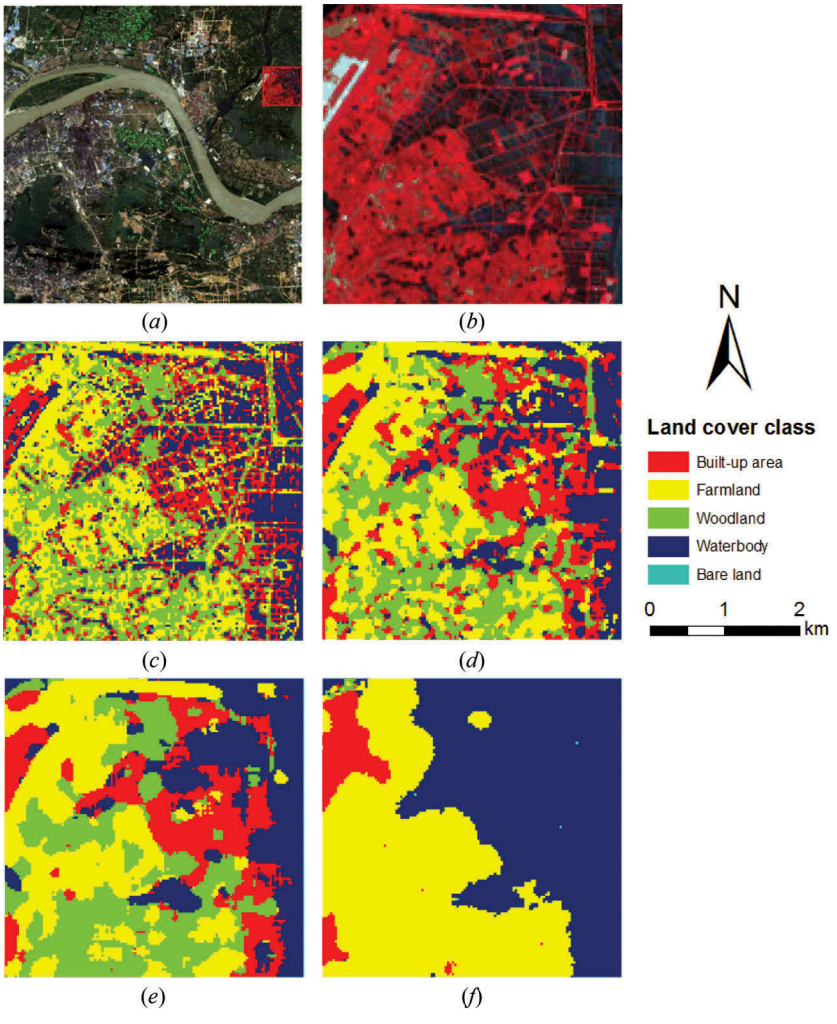

Figure 9. The Landsat 8 OLI true colour image of the study area (**a**), the enlarged false colour image of a subarea (**b**), corresponding NN pre-classification map (**c**), corresponding post-classification map by the majority spatial filter with a 3 × 3 window (**d**), corresponding post-classification map by the majority spatial filter with a 7 × 7 window (**e**), and corresponding optimal map of MCRF post-classification (**f**). The latitude and longitude of the upper left corner of the enlarged image are 30° 41′33″N and 114°38′06″E, respectively.

6. Conclusions

This study proved that, as a non-linear geostatistical method, the Bayesian MCRF cosimulation algorithm is an excellent method for improving accuracy of land cover classifications produced by conventional classifiers, when an expert-interpreted sample dataset is available for post-classification, even if the study area is relatively large and has a complex landscape. Five representative conventional classifiers (ML, NN, SVM, MD, and KM) were tested in this study; four are supervised methods, and one is a non-supervised method. The conventional classifiers achieved different land cover classification accuracies from the same remotely sensed image in pre-classifications, ranging from

67.1% (MD) to 81.9% (ML). However, the MCRF post-classification method made notable improvements in accuracy over all of the pre-classifications from the conventional classifiers, and the improvements range from 4.6% to 16.8%. In addition, most noise in the pre-classified maps was also removed by the post-classification operations. These improvements are mainly attributed to the MCRF cosimulation algorithm, which makes full use of spectral information (by pre-classified image data), expert knowledge and ancillary data (by sample data interpretation), and contextual information (by spatial correlation measurements).

One trade-off of the post-classifications by the MCRF method is that the smoothing effect in optimal classification land cover maps, brought by the MCRF cosimulation, removes most of linear features (mainly roads). However, even in the pre-classification maps, these linear features mostly are just partially captured road fragments and narrow striped objects (e.g. separating stripes in lakes for private fishery or lotus planting), therefore having little value for making schematic land cover/use maps. Considering that road network data are usually available from local transportation agencies, if they are needed in a land cover/use map, it is better to add the needed available road network data as a data layer to the final land cover map rather than to derive their fragments through classifying a remotely sensed image. Apparently, the other trade-off of the post-classification operation is the needed sample data interpretation process, which may be time consuming. These problems may be relieved by further efforts in algorithm development. For example, incorporating multiple-point statistics or other feature indices in the MCRF cosimulation algorithm may be helpful in capturing some linear features such as sharp river banks, and an automatic or semi-automatic method for accurate sample data interpretation may largely reduce the burden of expert interpretation. Nevertheless, the obvious accuracy improvement made by the MCRF method over conventional classifiers means that this post-classification method is promising in land cover classifications.

Acknowledgements

We thank the editors and anonymous reviewers for their constructive comments.

Disclosure statement

No potential conflict of interest was reported by the authors.

Funding

This research was supported in part by USA NSF [grant number 1414108].

References

Anderson, J. R., E. E. Hardy, J. T. Roach, and R. E. Witmer. 1976. *A Land Use and Land Cover Classification System for Use with Remote Sensor Data*. Washington, DC: US Geological Survey Professional Paper 964.

Barnsley, M. J., and S. L. Barr. 1996. "Inferring Urban Land Use from Satellite Sensor Images Using Kernel-Based Spatial Reclassification." *Photogrammetric Engineering and Remote Sensing* 62 (8): 949–958.

Brown, M., S. R. Gunn, and H. G. Lewis. 1999. "Support Vector Machines for Optimal Classification and Spectral Unmixing." *Ecological Modelling* 120 (2–3): 167–179. doi:10.1016/s0304-3800(99)00100-3.

Bruzzone, L., D. F. Prieto, and S. B. Serpico. 1999. "A Neural-Statistical Approach to Multitemporal and Multisource Remote-Sensing Image Classification." *IEEE Transactions on Geoscience and Remote Sensing* 37 (3): 1350–1359. doi:10.1109/36.763299.

Carvalho, J., A. Soares, and A. Bio. 2006. "Improving Satellite Images Classification Using Remote and Ground Data Integration by Means of Stochastic Simulation." *International Journal of Remote Sensing* 27 (16): 3375–3386. doi:10.1080/01431160600658099.

De Jong, S. M., T. Hornstra, and H.-G. Maas. 2001. "An Integrated Spatial and Spectral Approach to the Classification of Mediterranean Land Cover Types: The SSC Method." *International Journal of Applied Earth Observation and Geoinformation* 3 (2): 176–183. doi:10.1016/S0303-2434(01)85009-1.

Debeir, O., I. Van Den Steen, P. Latinne, P. Van Ham, and E. Wolff. 2002. "Textural and Contextual Land-Cover Classification Using Single and Multiple Classifier Systems." *Photogrammetric Engineering and Remote Sensing* 68 (6): 597–606.

Dobson, M. C., L. E. Pierce, and F. T. Ulaby. 1996. "Knowledge-Based Land-Cover Classification Using ERS-1/JERS-1 SAR Composites." *IEEE Transactions on Geoscience and Remote Sensing* 34 (1): 83–99. doi:10.1109/36.481896.

Goovaerts, P. 2002. "Geostatistical Incorporation of Spatial Coordinates into Supervised Classification of Hyperspectral Data." *Journal of Geographical Systems* 4 (1): 99–111. doi:10.1007/s101090100077.

Hsu, C.-W., and C.-J. Lin. 2002. "A Comparison of Methods for Multiclass Support Vector Machines." *IEEE Transactions on Neural Networks* 13 (2): 415–425. doi:10.1109/72.991427.

Kuemmerle, T., V. C. Radeloff, K. Perzanowski, and P. Hostert. 2006. "Cross-Border Comparison of Land Cover and Landscape Pattern in Eastern Europe Using a Hybrid Classification Technique." *Remote Sensing of Environment* 103 (4): 449–464. doi:10.1016/j.rse.2006.04.015.

Lambin, E. F., B. L. Turner, H. J. Geist, S. B. Agbola, A. Angelsen, J. W. Bruce, O. T. Coomes, R. Dirzo, G. Fischer, C. Folke, P. S. George, K. Homewood, J. Imbernon, R. Leemans, X. Li, E. F. Moran, M. Mortimore, P. S. Ramakrishnan, J. F. Richards, H. Skånes, W. Steffen, G. D. Stone, U. Svedin, T. A. Veldkamp, C. Vogel, and J. Xu. 2001. "The Causes of Land-Use and Land-Cover Change: Moving beyond the Myths." *Global Environmental Change* 11 (4): 261–269. doi:10.1016/s0959-3780(01)00007-3.

Lawrence, P. J., and T. N. Chase. 2010. "Investigating the Climate Impacts of Global Land Cover Change in the Community Climate System Model." *International Journal of Climatology* 30 (13): 2066–2087. doi:10.1002/joc.2061.

Li, W. 2007a. "Markov Chain Random Fields for Estimation of Categorical Variables." *Mathematical Geology* 39 (3): 321–335. doi:10.1007/s11004-007-9081-0.

Li, W. 2007b. "Transiograms for Characterizing Spatial Variability of Soil Classes." *Soil Science Society of America Journal* 71 (3): 881–893. doi:10.2136/sssaj2005.0132.

Li, W., and C. Zhang. 2007. "A Random-Path Markov Chain Algorithm for Simulating Categorical Soil Variables from Random Point Samples." *Soil Science Society of America Journal* 71 (3): 656–668. doi:10.2136/sssaj2006.0173.

Li, W., and C. Zhang. 2010. "Linear Interpolation and Joint Model Fitting of Experimental Transiograms for Markov Chain Simulation of Categorical Spatial Variables." *International Journal of Geographical Information Science* 24 (6): 821–839. doi:10.1080/13658810903127991.

Li, W., C. Zhang, D. K. Dey, and M. R. Willig. 2013. "Updating Categorical Soil Maps Using Limited Survey Data by Bayesian Markov Chain Cosimulation." *The Scientific World Journal* 2013: 1–13. doi:10.1155/2013/587284.

Li, W., C. Zhang, M. R. Willig, D. K. Dey, G. Wang, and L. You. 2015. "Bayesian Markov Chain Random Field Cosimulation for Improving Land Cover Classification Accuracy." *Mathematical Geosciences* 47 (2): 123–148. doi:10.1007/s11004-014-9553-y.

Li, X., Q. Meng, X. Gu, T. Jancso, T. Yu, K. Wang, and S. Mavromatis. 2013. "A Hybrid Method Combining Pixel-Based and Object-Oriented Methods and Its Application in Hungary Using Chinese HJ-1 Satellite Images." *International Journal of Remote Sensing* 34 (13): 4655–4668. doi:10.1080/01431161.2013.780669.

Loveland, T. R., B. C. Reed, J. F. Brown, D. O. Ohlen, Z. Zhu, L. W. M. J. Yang, and J. W. Merchant. 2000. "Development of a Global Land Cover Characteristics Database and IGBP Discover from 1 Km AVHRR Data." *International Journal of Remote Sensing* 21 (6–7): 1303–1330. doi:10.1080/014311600210191.

Lu, D., and Q. Weng. 2007. "A Survey of Image Classification Methods and Techniques for Improving Classification Performance." *International Journal of Remote Sensing* 28 (5): 823–870. doi:10.1080/01431160600746456.

Manandhar, R., I. O. Odeh, and T. Ancev. 2009. "Improving the Accuracy of Land Use and Land Cover Classification of Landsat Data Using Post-Classification Enhancement." *Remote Sensing* 1 (3): 330–344. doi:10.3390/rs1030330.

Mas, J.-F. 1999. "Monitoring Land-Cover Changes: A Comparison of Change Detection Techniques." *International Journal of Remote Sensing* 20 (1): 139–152. doi:10.1080/014311699213659.

Murai, H., and S. Omatu. 1997. "Remote Sensing Image Analysis Using a Neural Network and Knowledge-Based Processing." *International Journal of Remote Sensing* 18 (4): 811–828. doi:10.1080/014311697218773.

Park, N.-W., K.-H. Chi, and B.-D. Kwon. 2003. "Geostatistical Integration of Spectral and Spatial Information for Land-Cover Mapping Using Remote Sensing Data." *Geosciences Journal* 7 (4): 335–341. doi:10.1007/bf02919565.

Schmidt, K. S., A. K. Skidmore, E. H. Kloosterman, H. Van Oosten, L. Kumar, and J. A. M. Janssen. 2004. "Mapping Coastal Vegetation Using an Expert System and Hyperspectral Imagery." *Photogrammetric Engineering & Remote Sensing* 70 (6): 703–715. doi:10.14358/pers.70.6.703.

Shekhar, S., P. R. Schrater, R. R. Vatsavai, W. Wu, and S. Chawla. 2002. "Spatial Contextual Classification and Prediction Models for Mining Geospatial Data." *IEEE Transactions on Multimedia* 4 (2): 174–188. doi:10.1109/tmm.2002.1017732.

Stefanov, W. L., M. S. Ramsey, and P. R. Christensen. 2001. "Monitoring Urban Land Cover Change: An Expert System Approach to Land Cover Classification of Semiarid to Arid Urban Centers." *Remote Sensing of Environment* 77 (2): 173–185. doi:10.1016/s0034-4257(01)00204-8.

Tang, Y., P. M. Atkinson, N. A. Wardrop, and J. Zhang. 2013. "Multiple-Point Geostatistical Simulation for Post-Processing a Remotely Sensed Land Cover Classification." *Spatial Statistics* 5: 69–84. doi:10.1016/j.spasta.2013.04.005.

Thapa, R. B., and Y. Murayama. 2009. "Urban Mapping, Accuracy, & Image Classification: A Comparison of Multiple Approaches in Tsukuba City, Japan." *Applied Geography* 29 (1): 135–144. doi:10.1016/j.apgeog.2008.08.001.

US Geological Survey. 2012. "Frequently Asked Questions about the Landsat Missions." http://landsat.usgs.gov/band_designations_landsat_satellites.php

Vaiphasa, C., A. K. Skidmore, and W. F. De Boer. 2006. "A Post-Classifier for Mangrove Mapping Using Ecological Data." *ISPRS Journal of Photogrammetry and Remote Sensing* 61 (1): 1–10. doi:10.1016/j.isprsjprs.2006.05.005.

Van de Voorde, T., W. De Genst, and F. Canters. 2007. "Improving Pixel-Based VHR Land-Cover Classifications of Urban Areas with Post-Classification Techniques." *Photogrammetric Engineering and Remote Sensing* 73 (9): 1017.

Wilkinson, G. G. 2005. "Results and Implications of a Study of Fifteen Years of Satellite Image Classification Experiments." *IEEE Transactions on Geoscience and Remote Sensing* 43 (3): 433–440. doi:10.1109/tgrs.2004.837325.

Zhang, Y. 1999. "Optimisation of Building Detection in Satellite Images by Combining Multispectral Classification and Texture Filtering." *ISPRS Journal of Photogrammetry and Remote Sensing* 54 (1): 50–60. doi:10.1016/s0924-2716(98)00027-6.

Zhang, Y. 2001. "Detection of Urban Housing Development by Fusing Multisensor Satellite Data and Performing Spatial Feature Post-Classification." *International Journal of Remote Sensing* 22 (17): 3339–3355. doi:10.1080/01431160010031289.